New radio data for the radio galaxies from the Big Trio program

O. Zhelenkova[1] · A. Temirova[2] · Yu. Parijskij · N. Soboleva

[1] Special Astrophysical Observatory of the Russian Academy of Sciences, Nizhny Arkhyz, 369167 Russia

[2] St. Petersburg Branch of the Special Astrophysical Observatory of the Russian Academy of Sciences, St. Petersburg, 196140 Russia

DOI: 10.26119/2025-moc04 EDN: ovapur
eLocator: moc04

Abstract. The Big Trio program, based on steep and ultra-steep spectrum sources from RATAN-600 Cold Experiment surveys, targeted distant radio galaxies. New multiwavelength surveys enabled indepth analysis of 113 sources to determine their evolutionary status, environmental characteristics, and long-term spectral changes. Analysis revealed that 20 % show signs of initial, fading, or resumed activity. Twenty four sources reside in galaxy groups/clusters or show jet reorientation; four paired sources have parent galaxies just tens of kpc apart. Spectral index analysis ($\alpha \leq -0.9$) showed a declining trend: 90 sources (out of 113) met the criterion in the 365–3940 MHz range (pre-1996 data), dropping to 70 in 340–3000 MHz (modern surveys) and 39 in 76–226 MHz (GLEAM). This decrease stems from instrumental effects (angular resolution differences affecting flux density measurements) and improved low-frequency spectral characterization. For individual sources, spectral index variations may also reflect intrinsic evolutionary processes and source variability.

Keywords: active galaxies: high-redshift radio galaxies; general radio continuum

1. Introduction

Radio galaxies with redshift $z > 2$ and luminosity at 500 MHz $L_{500} > 10^{27}$W·Hz^{-1} are distinguished as a separate population of high-redshift radio galaxies (HzRG) (Miley & De Breuck 2008).

The components of the HzRG radiation are the emission of dust, stars, and an active nucleus. Studies of the first two components show that HzRGs belong to the most massive stellar systems in the early Universe (Seymour et al. 2007; Bryant et al. 2009; De Breuck et al. 2010) and demonstrate signs of a massive galaxy at the stage of formation (Miley & De Breuck 2008), as well as rapid accretion of matter onto a supermassive black hole (SMBH) (Carilli et al. 1997; Vernet et al. 2001; Nesvadba et al. 2008; Drouart et al. 2012). The powerful submillimeter emission is also directly related to active star formation (Rawlings et al. 2013). The dust torus of the radio galaxy obscures the light from the hot accretion disk and provides more opportunities to study the stellar population of the host galaxy than in the case of the quasar (Hopkins & Beacom 2006; Aird et al. 2010).

There is a reason to believe that the galaxy and the SMBH are formed simultaneously (Magorrian et al. 1998; Haring & Rix 2004; Hopkins et al. 2006). According to the hierarchical model, the most massive star systems form at peaks of dark matter density by merging of large numbers of small galaxies (White & Rees 1978). At $z \gtrsim 2 - 2.5$, galaxy clusters are still in the process of forming, as there is not enough time to virialize. For this reason, they are called protoclusters. Observations show that HzRGs are most often found in fairly dense environments (Stevens et al. 2003; Falder et al. 2010; Stevens et al. 2010; Galametz et al. 2012; Mayo et al. 2012), and protoclusters are likely to be found in their immediate vicinity. Since HzRGs are found at high redshifts, they may mark galaxy clusters at cosmological distances.

Bright radio galaxies at $z > 6$ can be used to study the reionization process in detail (Saxena et al. 2018a). The red-shifted $\lambda = 21$ cm (1.4 GHz) ultra-fine transition line of neutral hydrogen falls within the low-frequency radio range ($\nu < 200$ MHz) and can be observed as absorption in the spectra of the radio galaxy at $z > 6$ (Carilli et al. 2002). Such absorption lines can, in principle, be detected by current and next-generation radio telescopes (Saxena 2019).

Blind search for distant radio galaxies is not effective. At high redshifts, identifying the host galaxy and determining its properties requires a large investment of observing time, and is often beyond the reach of most existing instruments.

Tielens et al. (1979) discovered that distant radio sources have steep spectra. It was confirmed in subsequent studies, for example, Kapahi & Kulkarni (1990). Although steep spectra are also observed in pulsars and dying radio galaxies, this criterion is often used in the selection of distant radio galaxy candidates. The effectiveness of this approach was demonstrated by Roettgering et al. (1994, 1997); De Breuck et al. (2000, 2004, 2006); Broderick et al. (2007). Additional criteria are also used — small angular sizes, quite a weak integrated flux density, the absence of candidates in the optical and infrared ranges, as well as the shape of the spectrum — a convex spectrum at low frequencies. Similar criteria were used in Saxena et al. (2018b), where a radio galaxy with $z = 5.72$ was found in their sample, which is currently the most distant radio galaxy.

The Big Trio program. In the SAO RAS, the Big Trio program (Goss et al. 1992b; Parijskij et al. 2000) was launched in the early 1990s aimed at searching for distant radio galaxies and their further study. The selection of objects was made from radio sources discovered in the Cold experiment[1] and included in the RC (RATAN Cold) catalog (Parijskij et al. 1991; Pariiskij et al. 1992).

[1]The Cold experiment (Berlin et al. 1981, 1984a,b) consisted of series of long-term surveys of a wide sky strip ($24^h \times 0.7°$) at the declination of microquasar SS 433 ($\delta \approx 5°$) at several frequencies, have been carried out in 1980-1987. The aim of the surveys was the search for cosmic microwave background fluctuations. The deepest flux density limit ($\simeq$2.5 mJy) had been reached at 3.94 GHz.

The main selection criterion was the steepness of the radio spectrum ($\alpha \leq -0.9$). The two-frequency spectral indices of the sources were determined using data from RC (3.94 GHz) and UTRAO (365 MHz) (Douglas et al. 1980), which was one of the early releases of the Texas Sky Survey. Additional criteria were also used – flux density (not brighter than several hundred millijansky at 3.94 GHz), double radio sources of small angular sizes (LAS $< 20''$) (Kopylov et al. 1995).

For the SS (Steep Spectra) sample sources, the radio coordinates were refined, the morphological structure and angular sizes were determined using the observations available in the MIT-GB-VLA archive (Fletcher et al. 1996), and observations were also carried out using the VLA for other sources from the RC catalog (Parijskij et al. 1995). In total, 389 radio maps were obtained for 208 RC sources at a frequency of 1.4 GHz with an angular resolution from $1.5''$ to $4.5''$. Some of the unresolved objects were observed at frequencies of 4.8–14 GHz with a resolution of $0.4''$.

Within the framework of the Big Trio program in 1991–2003, 113 objects were observed with the 6-meter optical telescope BTA. In addition, frames for 22 radio sources with subsecond visibility were obtained using the 2-meter NORDIC telescope (Pursimo et al. 1999). For most sources (94 %) of the SS sample, optical companions were found at a limiting magnitude of $m_R \approx 24.5^m$ (Goss et al. 1992a; Kopylov et al. 1995; Parijskij et al. 1996). Based on BVRI photometry, photometric redshift estimates were made for 48 % of the sample (Verkhodanov et al. 2002a).

Spectroscopic studies of parent objects were carried out using the BTA with the SCORPIO focal reducer (Afanasiev& Moiseev 2005). Spectra were obtained for 71 objects (Dodonov et al. 1999; Afanasiev et al. 2003; Kopylov et al. 2006; Parijskij et al. 2010). 50 % of the hosts were classified as radio galaxies according to the type of optical spectrum (narrow emission lines), and half of them have $z > 1$. A quarter of the hosts were classified as quasars (broad spectral lines), 70 % of which have $z > 1$. No lines were detected in the spectra of the remaining quarter of candidates due to the weak brightness of the objects in optical band.

Among 54 radio sources with measured spectral redshifts, 5 galaxies and 5 quasars with $z > 2$ were discovered, including two sources with $z > 3$ and one with $z > 4$. The last three sources with $z > 3$ have extreme radio luminosities at 500 MHz $L_{500} > 10^{28}\mathrm{W}\cdot\mathrm{Hz}^{-1}$. Currently, RC J0311+0507, $z = 4.514$ (Kopylov et al. 2006; Wang et al. 2021), is one of the two most powerful known radio galaxies, along with 8C 1435+635, with a luminosity of $L_{150} > 10^{30}\mathrm{W}\cdot\mathrm{Hz}^{-1}$ (Saxena et al. 2018b).

The sample of the Big Trio program has been studied quite well. With the advent of deep sky surveys, it became possible to confirm or refine optical identifications, understand the morphology of the radio source, refine the radio spectra, etc.

The paper adopts the flat ΛCDM cosmology based on Planck's results: $H_0 = 67.4\,\mathrm{km}\cdot\mathrm{s}^{-1}\mathrm{Mpc}^{-1}$, $\Omega_m = 0.315$ (Planck Collaboration 2020). The spectral index of the radio source α is defined as $S_\nu \propto \nu^\alpha$.

2. Used information resources and software

To study radio sources, we took information from the surveys VLSSr (Lane et al. 2014), TGSS (Intema et al. 2017), GLEAM (Hurley-Walker et al. 2017), VCSS (Polisensky et al. 2016; Peters et al. 2021), TXS (Douglas et al. 1996, 1980), MRC (Large et al. 1991), RACS (Hale et al. 2021; Duchesne et al. 2024), NVSS (Condon et al. 1998), FIRST (Helfand et al. 2015), VLASS (Gordon et al. 2023), RC (Parijskij et al. 1991; Pariiskij et al. 1992), PMN (Wright et al. 1994), GB6 (Gregory et al. 1996), PKS (Wright & Otrupcek 1990).

To clarify the morphological structure of radio sources, in addition to the existing collection of data obtained on the VLA for the Big Trio program (Parijskij et al. 1996), we looked through the radio maps from the GLEAM, TGSS, RACS, FIRST, VLASS surveys, and the NRAO archive.

To work with catalogs and surveys, the Aladin Sky Atlas software (Bonnarel et al. 2000) was used, as well as to work with tables — TOPCAT (Taylor 2005).

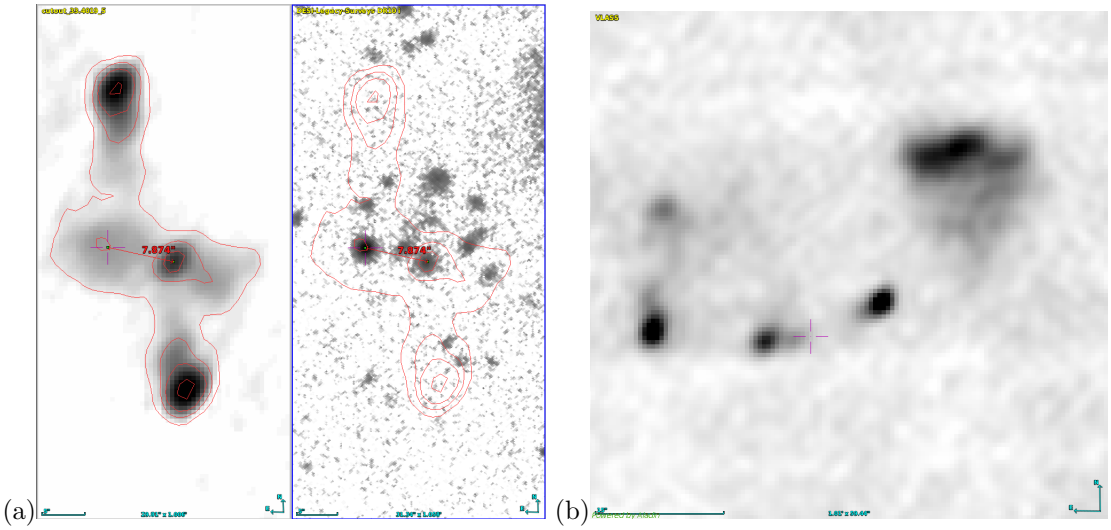

Figure 1. Examples of radio sources: a) X-shaped radio source RC J0213+0516. Near its host galaxy (z_{sp}=0.935) there is a quasar (z_{sp}=0.934) associated with a weak radio source. The distance between the galaxy and the quasar is 7.9″ or 61 kpc; b) RC J0519+0510 is a DDRG-type radio source, which can also be classified as a rare morphological type of HSR sources.

The radio spectra were plotted using the spg program from the FADPS data processing package (Verkhodanov et al. 1993) .

To search for information about the radio sources, we used the SIMBAD (Wenger et al. 2000), VizieR, CATS (Verkhodanov et al. 2005), NED, DataLab (Huang et al. 2020) databases, as well as the optical surveys LS, DES (Abbott et al. 2018, 2021), HSC-SPP (Aihara et al. 2019, 2022), including near- and mid-infrared surveys LAS UKIDSS (Lawrence et al. 2007), GPS UKIDSS (Lucas et al. 2008) and WISE (Cutri et al. 2012; Marocco et al. 2021).

3. Morphological structure of radio sources

Based on the morphological structure of a radio source, it is possible to determine its evolutionary status — young, active, fading, as well as its environment.

For half of SS-sources, there are VLA observations with an angular resolution of $0.1'' \div 2.38''$ (Fletcher et al. 1996; Parijskij et al. 1995), and for the other half, there are maps from the VLASS survey with an angular resolution of 2.5″. For the radio source RC J0311+0507 (4C 04.11), MERLIN and EVN maps with an angular resolution of 0.025″ (Parijskij et al. 2014) were obtained, and for RC J1740+0502, MERLIN maps with an angular resolution of 0.1″.

According to these radio maps, point unresolved radio sources make up 18 % of the sample, with 9 of them being point sources on the VLASS maps and 11 unresolved on maps with an angular resolution of $0.4'' \div 1.6''$. For 44 double sources, the morphology was determined from the VLASS maps, and for 49 — from maps with an angular resolution of $0.025'' \div 2.38''$.

Visual examination of radio maps and cutouts from the DESI, DES, HSC-SSP optical surveys, including the LAS UKIDSS and WISE infrared surveys, revealed that some radio sources are not single but consist of two sources located close to each other in the picture plane.

There were six such sources. Moreover, each of RC J0126+0502, RC J0213+0516, RC J0318+0506, and RC J1251+0446 forms a pair of close radio sources with angular distances between the parent galaxies of about $6'' - 8''$ or about 50–70 kpc.

In the NVSS and TGSS radio surveys, the sources RC J0318+0456 and RC J0324+0442 are double radio sources. Higher angular resolution maps and optical data have shown that each

component of the radio sources RC J0318+0456 and RC J0324+0442 are actually independent sources that happen to be in the line of sight.

As an example of a pair of radio sources, we consider RC J0213+0516 (Fig. 1a), where the galaxy SDSS J021336.32+051819.0 is the host of a double X-shaped radio source with the coordinates of the core $\alpha_{2000} = 02^h12^m36.32^s$ and $\delta_{2000} = +05°18'18.8''$. It has a redshift of $z_{\rm sp}$=0.935 (Parijskij et al. 2010). The quasar SDSS J021336.80+051820.7 has $z_{\rm sp}^{\rm SDSS}$=0.934 and is associated with the weak radio source with coordinates $\alpha_{2000} = 02^h13^m36.77^s$ and $\delta_{2000} = +05°18'20.7''$. The angular distance between the hosts is 7.9″ or 61 kpc.

Among the double radio sources, there are sources that cannot be classified as either FRI or FRII (Fanaroff & Riley 1974). They are classified as FRI/FRII or HyMoRS (HYbrid MOrphology Radio Sources) (Gopal-Krishna & Wiita 2000; Kapinska et al. 2017; Stroe et al. 2022).

Radio galaxies with double lobes DDRG (Double-double Radio Galaxy) (Schoenmakers et al. 2000; Saikia et al. 2006) also do not quite fit into the FRII type. In the SS sample, we classified six radio sources as the hybrid type and three radio sources as the DDRG type. An example of a double-double radio source RC J0519+0510 is shown in Fig. 1b.

37 (27 %) double sources have a core, and for 16 of them the contribution of the core to the total flux density at 3 GHz is less than 5 %, and for 15 sources with a core this contribution can be from 10 % to 60 %. We classified double sources with a core for which the contribution of the core to the total flux density at 3 GHz is more than 10 % as triple sources. In addition, for 6 radio sources, the contribution of the core is more than 35 %, and they can be classified as CDT (Core-Dominated Triple) (Marecki et al. 2006).

There are radio sources with deformed lobes. They are classified into the following types — winged sources WRG (Winged Radio Galaxy)[2] (Cohen et al. 2007; Yang et al. 2019; Bera et al. 2022), "head-tail" radio sources HT (Head-tailed)[3](Rudnick & Owen 1976; Blanton et al. 2000; Missaglia et al. 2019; Sasmal et al. 2022), as well as recently discovered radio sources with a ring-shaped diffuse radio emission — ORC (Odd Radio Circle) (Norris et al. 2021) and HSR (Horseshoe-Shaped Ring) (Kumari & Pal 2024).

In the SS sample, we classified 12 WRGs, 8 WAT sources, and two more sources that are C-shaped or even horseshoe-shaped (HSR). RCJ0519+0510 is shown in Fig. 1b as an example.

The sample included two giant radio galaxies (Willis et al. 1974; Lara et al. 2001; Andernach et al. 2021) — RC J0152+0453 and RC J1333+0451 with projected linear sizes of 990 and 1100 kpc, respectively, as well as twenty-six compact radio sources with sizes from 0.7 to 19 kpc or with an angular size less than 3″, if the redshift is not known for the host of the unresolved radio source.

4. Analysis of total flux densities and spectral indices

Using a representative set of flux density measurements, we calculated spectral indices for each source in the SS sample. The calculations utilized a linear fit to flux densities across three different datasets, covering the following frequency ranges: 365–3940 MHz (data prior to 1996), 340–3000 MHz (from recent catalogs), and 76–227 MHz (GLEAM survey data). A comparative analysis of the results revealed a systematic decrease in the proportion of sources with spectral indices satisfying the condition $\alpha < -0.9$.

When linearly fitting flux densities, the edge points of the spectral indices can have a significant impact on the resulting indices, especially with a limited number of data points. To address this issue, we conducted a targeted comparison of old and new measurements at frequencies of 365 MHz (TXS) versus 340 MHz (VSSS) and 1400 MHz (NVSS) versus 1368 MHz (RACS). According

[2]WRG include X-, S-, Z-shaped radio galaxies (XRG, ZRG).

[3]HT galaxies include WAT (Wide-Angle Tailed), NAT (Narrow-Angle Tailed) and C-shaped radio galaxies.

to established astrophysical concepts, sources with steep spectra typically exhibit greater temporal stability than sources with flat spectra.

To identify sources with significant discrepancies between measurements, we implemented a two-step procedure: first, we calculated the variability index for each source; second, we performed a detailed analysis of sources with variability indices greater than 3. This threshold allows us to select objects with significant discrepancies between the data points. Particular attention was paid to the data at 340 and 365 MHz, as these frequencies are important in determining spectral steepness. Refining the flux densities at these frequencies allows for a more accurate interpretation of the observed decrease in the number of sources with $\alpha < -0.9$. This analysis proves the importance of separating instrumental effects from properties of sources.

4.1. Variability indices

For the vast majority of sources in the sample, there is sufficient data to compare integrated flux densities over two or more epochs. We compared fluxes at 340–365 MHz (VCSS, TXS), 1368–1400 MHz (RACS-mid, NVSS), 3900–3940 MHz (GAISh, Cold), and 4850–5000 MHz (MIT-GB, GB6, PMN, PKS).

The time interval between the observations of the VCSS and TXS surveys is about 40 years, if the average value between the year of the beginning and the end of the survey is taken as the observation epoch. The interval between the average epochs of the RACS-mid and NVSS surveys is 27 years. The interval between the observations of one source in the Zelenchuk-GAISh survey (Amirkhanyan et al. 1985) and the series of Cold surveys can be from 2 to 19 years. In surveys MIT-GB (Bennett et al. 1986), GB6 (Gregory et al. 1996), PMN (Griffith et al. 1995) and PKS (Shimmins et al. 1974; Binette et al. 1981) the interval between observations can be up to 18 years. Note that data for 340–365 MHz are available for 77 % of the sample, for 1368–1400 MHz – 100 %, 3940 MHz – 89 %, 4850 MHz – 82 %.

We calculated several variability indices using a simple variability criterion:
$\mathrm{V}=(S_{\max} - S_{\min})/\sqrt{\sigma^2_{\max} + \sigma^2_{\min}} > 3$,
where $S_{\max}$, $\sigma_{\max}$ and $S_{\min}$, $\sigma_{\min}$ are the maximum and minimum flux densities and their measurement errors, respectively. In a such way the variability indices V_{3940} for 3900–3940 MHz and V_{4850} for 4775–5000 MHz have been calculated.

The variability index V_{340} for frequencies of 340 and 365 MHz according to VCSS and TXS data, as well as the index V_{1400} for 1368 and 1400 MHz according to RACS-mid and NVSS data, was determined as follows:
$V_{340} = (S_{340} - S_{365})/\sqrt{\sigma^2_{340} + \sigma^2_{365}}$,
$V_{1400} = (S_{1368} - S_{1400})/\sqrt{\sigma^2_{1368} + \sigma^2_{1400}}$,
since it was interesting to compare where S_{340} is greater than S_{365} and vice versa. For this reason, negative values appeared for V_{340} and V_{1400}.

The variability indices distributions V_{340} and V_{1400}, V_{3940} and V_{4850} are shown in the Fig. 2a, Fig. 2b, respectively. The significant difference between the distributions of the indices V_{340} and V_{1400} turned out to be unexpected, with all 113 radio sources in the sample having a variability index $|V_{340}| < 3$.

Of the 87 sources for which data is available in the VCSS and TXS catalogs, 44 % have $|V_{340}| > 3$. At frequencies of 3900–3940 MHz, of the 101 radio sources, 31 % have $V_{3940} > 3$, and at 4850–5000 MHz, of the 93 objects, 37 % have $V_{4850} > 3$. For 47 radio sources, at least one of V_{3940} and V_{4850} is greater than 3; for 10 radio sources, both indices are greater than 3. And for 4 sources, RC J0934+0505, RC J1142+0455, RC J1456+0456, and RC J2225+0523, all three indices $|V_{340}|$, V_{3940}, and V_{4850} are greater than 3.

Next, we will try to figure out why there is such a difference between the variability index V_{340} and V_{1400}.

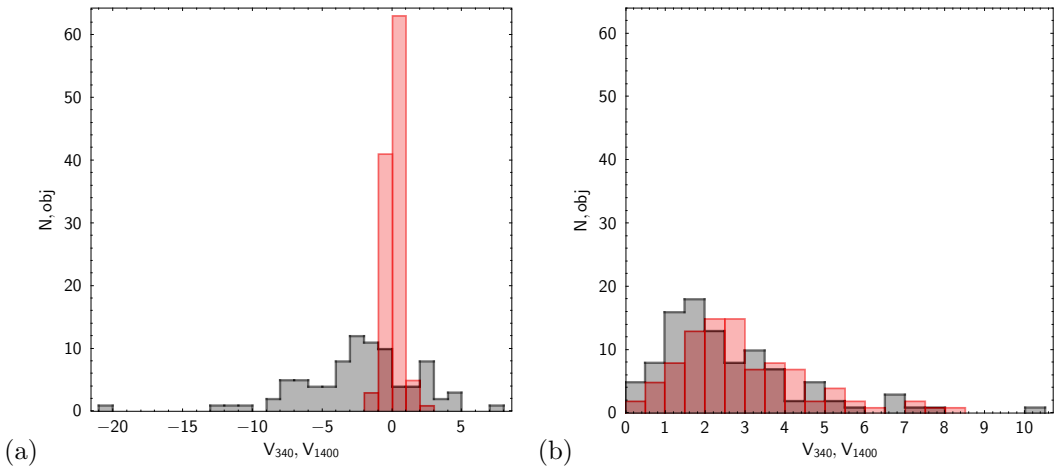

Figure 2. The variability indices distribution: (a) V_{340} (grey) and V_{1400} (red); (b) V_{3940} (grey) and V_{4850} (red).

4.2. Flux density measurement errors

We inspected the vicinity of the radio sources using cutouts from the GLEAM, TGSS, RACS-low, and RACS-mid surveys, which were checked for the presence of the radio sources close to the object under investigation, which could make an additional contribution to the value of S_{365}, as well as other reasons that could affect the value of S_{340}.

4.2.1. Contribution from nearby radio sources

Note that Douglas et al. (1996) indicated that two sources of comparable brightness would be resolved in the TXS catalog if they were separated by $> 9.6'$ in right ascension or by $> 8.1'$ in declenation. Trying to account for the contribution from nearby radio sources to S_{365} for the object under study, we chose a search area of approximately the same size. Using the RACS-low cutouts, we counted the sources that fell into the area, summed up their flux densities, and determined their total fraction relative to the source under study, which was then taken into account in S^c_{365} by subtracting this fraction from the total flux density S_{365}. For 16 out of 87 radio sources, neighboring sources were not detected in the studied regions.

The histogram in Fig. 3a shows the distributions of variability parameters V_{340} (grey) and V^c_{340} (red) for sources with neighbors. The parameter V^c_{340} takes into account the contribution of neighboring sources to the integral flux density S_{365}. The average value of the variability index is $V_{340} = -2.38$; and after correction for the contribution of neighbors, it became $V^c_{340} = -0.56$.

4.2.2. Errors of flux determination for double radio sources

From the sources with VCSS data, we selected double sources with angular sizes $LAS > 15''$, exceeding the angular resolution of the VCSS survey. The LAS angular size (the largest angular size) was measured from the outer VLASS components of the radio source. The sample included 28 double sources with angular sizes in the range of $15'' \div 124''$.

As it turned out, the integral flux density of some sources in the VCSS catalog is not always determined correctly. This is especially true for sources with asymmetric flux density components, according to the maps of the FIRST and VLASS surveys. Such radio sources can be represented in VCSS by a single component, and then the integral flux density S_{340} turns out to be underestimated. Note that only two sources out of 28 double radio sources have two components in the VCSS catalog — RC J0318+0456 ($LAS = 77.7''$) and RC J1148+0455 ($LAS = 40.5''$).

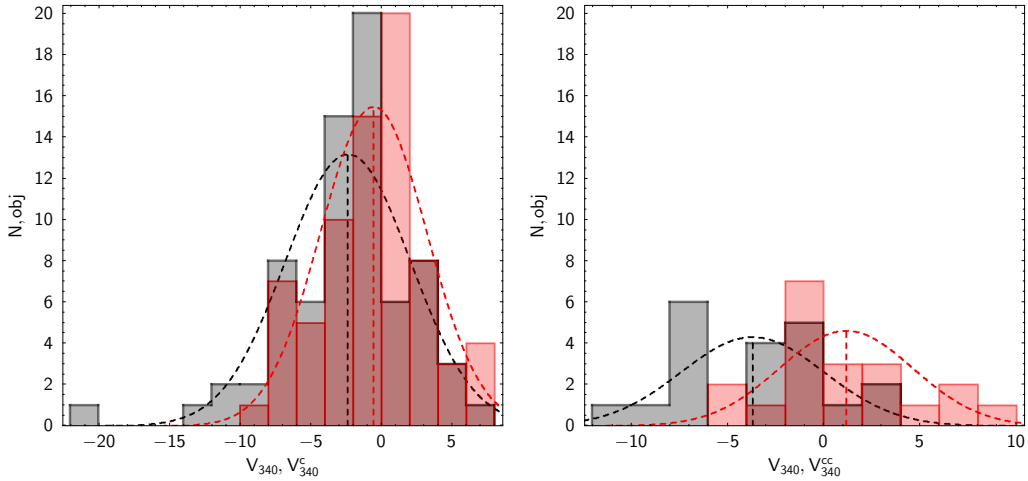

Figure 3. Diagrams showing the distribution of variability indices (a) V_{340} (marked in grey) for sources with neighbors, and V^c_{340} (in red), where the contribution from neighbors is taken into account; (b) for double sources V_{340} (grey) and V^{cc}_{340} (red). The index V^{cc}_{340} takes into account both the underestimated flux S_{340} of double radio sources and the contribution from neighbors. The Gaussian approximation of the quantities is shown by the dashed lines in black and red, respectively.

As a result, for 11 double radio sources with $LAS > 15''$, when correcting the integrated flux density of S_{340} using data from other radio catalogs, the value of S^{cc}_{340} was increased by $7\% \div 50\%$ compared to S_{340}. As a result, their variability indices in absolute value decreased and became less than 3. Figure 3b shows histograms showing the distributions of V_{340} (grey) and V^{cc}_{340} (red) for the double radio sources. When calculating the index V^{cc}_{340}, the contribution from nearby sources to the value of S_{365} was taken into account, as well as the correction of the flux density S_{340} for double radio sources.

The average value of the variability index of double sources was $V_{340} = -3.70$, and after correction of the underestimation of the integral flux densities, it became $V^{cc}_{340} = 1.15$.

Nevertheless, after these corrections, the variability index for double radio sources RC J1031+0443, RC J1142+0455, RC J2029+0456, and RC J2036+0451 remained at the level of $|V^{cc}_{340}| > 3$. We believe that the value of the variability index V_{340} for these double radio sources is overestimated, since we failed to correct the underestimated flux density S_{340}.

There are two possible reasons for the underestimation of the integrated flux density S_{340}. One of them is the peculiarities of the procedure for processing double sources with LAS $> 15''$ in the VCSS survey; the second is the presence of extended low surface brightness emission, which is not recorded in VCSS but can make an additional contribution to the integrated flux density in the GLEAM and TXS surveys.

4.3. Radio sources with $|V^c_{340} > 3|$

If we discard the sources for which the contribution to the flux density S_{365} from nearby sources is taken into account, then 19 sources with $|V^c_{340}| > 3$ remain. The parameters of these sources are presented in Table 1. The type and magnitude of the parent object were determined from the LS survey, the redshift — Parijskij et al. (2010), SDSS, LS.

The Table 1 presents the parameters of three groups of radio sources: 5 sources with a peak in the spectrum in the range 100–500 MHz, 6 sources with $V^c_{340} > 3$ and 9 with $V^c_{340} < -3$. Eight sources in the sample have a peak in the radio spectrum at frequencies of 100–500 MHz. Five of them have VCSS survey data. Four sources have $V^c_{340} < -3$, and one source, RC J0133+0459, has $V^c_{340} < 3$. All five sources have small angular sizes (see Table 1) and are not resolved in the VLASS survey. The parent objects are faint galaxies of 23–25 magnitudes in optical band, except for the quasar RC J1100+0444.

Table 1. Parameters of radio sources with a significant variability index. Name — radio source; V^c_{340}, V_{3940}, V_{4850} — variability indices at 340, 3940 and 4850 MHz; Type — the type of the host: Q — quasar, G — galaxy, EF — empty field; mag_r — the magnitude in the r-filter; LAS — the angular size; Maj — the major axis of the source in VLASS; RType — the type of the radio source: P — point, D — double, T — triple, cdt — triple with dominant core, css — compact radio source with steep spectrum; z — the redshift; mz — "s" — spectroscopic z, "p" — photometric z. A sign "?" indicates an uncertain type definition. Sources marked with "*" are presumably variable in terms of total flux density.

Name	V^c_{340}	V_{3940}	V_{4850}	Type	mag_r	LAS, $''$	Maj, $''$	Rtype	z	mz
Peaked-spectrum radio sources										
1. RC J0133+0459	2.7	0.1	1.7	G?	25.1	0.2	3.3	P		
2. RC J0250+0512	-9.8	2.6	3.9	EF	>25	1.2	2.9	D/css		
3. RC J0907+0439	-5.7	5.0	1.8	G?	24.7	0.3	2.8	P		
4. RC J1100+0444*	-3.1	4.8	1.8	Q	19.1	0.3	2.8	P	0.886	s
5. RC J1150+0459	-4.8	1.7	2.6	G?	23.3	0.3	2.9	P	1.27	s
Radio sources with $V^c_{340} > 3$										
1. RC J0135+0450*	3.5	-	1.5	Q?	18.6	7.8	7.7	T/cdt	0.372	s
2. RC J0143+0505*	4.1	-	4.2	Q	20.8	7.4	7.4	T	2.135	s
3. RC J1456+0456*	7.2	3.5	3.1	Q	20.1	2.2	3.2	P	2.136	s
4. RC J1503+0456*	4.9	1.7	1.2	Q?	22.9	4.5	4.5	T/cdt	0.788	s
5. RC J1551+0458*	3.1	1.0	1.2	G	23.9	11.6	11.5	D	1.29	p
6. RC J1703+0502	4.1	0.8	2.8	G?	23.8	1.8	3.4	D/css	1.23	p
Radio sources with $V^c_{340} < -3$										
1. RC J0034+0513	-6.5	1.5	1.8	G	23.1	12.1	12.2	T?	0.962	s
2. RC J0226+0512*	-7.6	2.6	1.9	Q	20.1	10.7	19.8	D;dd	1.242	s
3. RC J0311+0507	-5.8	1.3	2.9	G	22.9	2.8	17.4	D;mc	4.508	s
4. RC J0355+0449	-4.8	1.4	7.7	G?	24.1	2.4	18.6	D;css	2.7	p
5. RC J0934+0505	-5.2	3.1	7.0	G?	23.0	5.0	17.7	D	1.68	p
6. RC J1011+0502	-4.0	1.6	2.1	G?	23.8	2.8	20.0	D;css		
7. RC J1124+0456*	-7.6	2.7	3.7	G	17.3	11.9	-	D;mc	0.284	s
8. RC J1154+0431*	-3.6	1.2	2.0	Q	19.3	6.7	20.4	D	0.988	s
9. RC J2225+0523*	-3.8	4.9	4.4	Q	17.8	2.7	17.9	T	2.323	s

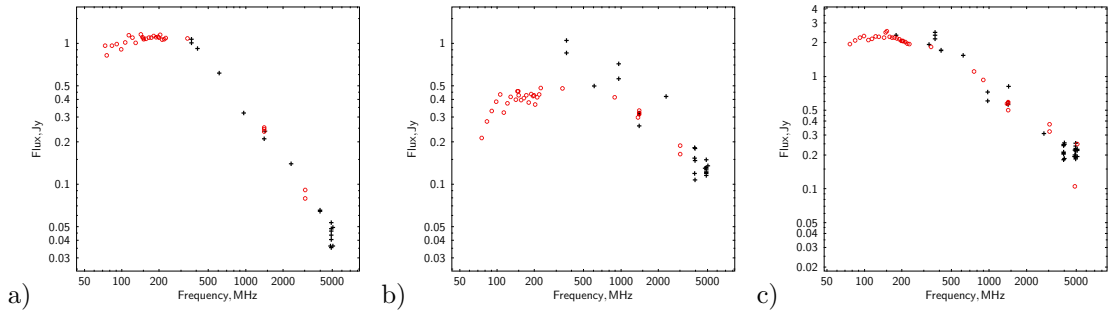

Figure 4. Radio spectra of sources with a spectral peak: (a) RC J0133+0459, (b) RC J0907+0439, (c) RC J1100+0444, constructed using data from Bursov et al. (1996) and new data from GLEAM, VCSS, RACS, VLASS (marked in red).

Orienti & Dallacasa (2021) noted that during the adiabatic expansion of homogeneous synchrotron sources, a shift of the spectral peak towards low frequencies can be observed in the continuum spectrum.

The radio spectra of the MPS sources RC J0133+0459, RC J0250+0512, RC J0907+0439, RC J1100+0444, and RC J1150+0459 are shown in Fig. 4. Of these sources, no spectrum shift is observed for RC J0133+0459 (Fig. 4a), while for RC J0907+0439 such shift is most noticeable (Fig. 4b). The quasar RC J1100+0444 (Fig. 4c) is a variable source that may exhibit a peak in the spectrum during periods of activity.

We suggest that the lower flux density S_{340} compared to S_{365} for these MPS sources, excluding RC J1100+0444, is due to a shift of the spectral peak caused by the radio source expansion, which was noticeable in the TXS and VCSS data over an interval of 34÷48 years between the observing epochs of these surveys.

Nine sources with $V^c_{340} < -3$ (see Table 1) have small angular sizes LAS $< 8''$. Four of them have quasars as their parent objects and are most likely variable objects. The remaining five objects are even smaller in angular size and are presumably young sources and exhibit a shift of spectral maximum to low frequencies in their spectrum, like MPS sources. Together with MPS sources, including those without data in the VSSS, these 13 sources (12 % of the sample) are young.

Thus, the presence of a large proportion of objects with $|V_{340} > 3|$ among the sample sources is explained, first of all, by the difference in the angular resolution of the surveys and the contribution to the integral flux density of S^o_{365} close sources, as well as the underestimated value of S_{340} for some double sources.

Ultimately, we concluded that sources with $|V_{340} > 3|$ may include young, rapidly evolving sources, variable sources, and sources with an extended low-surface-brightness component, likely generated by a previous episode of activity in radio band. For such sources, the extended component may not be detected in the VCSS, but is more likely to be detected in the TXS and GLEAM.

The Table 1 shows 10 sources: RC J0135+0450, RC J0143+0505, RC J0226+0512, RC J1100+0444, RC J1124+0456 (4C+05.50), RC J1154+0431, RC J1456+0456, RC J1503+0456, RC J1551+0458 and RC J2225+0523, which we classified as variables based on the available data. Note that when searching for variable sources in the Cold experiment surveys, RC J0506+0508, RC J1124+0456, RC J1213+0500, RC J1551+0458 were marked as variable radio sources (Majorova & Zhelenkova 2012; Majorova et al. 2015). As a result, 12 radio sources, which is at least 11 % of the sample, exhibit total flux density variability.

5. Spectral indices of sources of the SS-sample

The initial selection of candidates for the sample of sources with steep spectra was made by the two-frequency spectral index $\alpha^{\rm RC}_{\rm UTR} \le -0.9$ at frequencies of 365 and 3940 MHz using the integral flux densities from the UTRAO and RC (Soboleva et al. 1994) catalogs. And according to the data of this publication, 94 % of the sources in the sample that we study have $\alpha^{\rm RC}_{\rm UTR} \le -0.9$.

We compared the spectral indices of the SS sample sources obtained from the spectra constructed by approximating data from several sets of integrated flux densities.

We calculated spectral indices for the following data sets:

"old": Spectral index α^{3940}_{365} at 365 and 3940 MHz is determined by a linear approximation of the data from Bursov et al. (1996), which contains the most complete collection of measurements obtained before 1996, as well as from observations performed on RATAN-600 (Parijskij et al. 1991; Pariiskij et al. 1992; Soboleva et al. 1994; Bursov 1996; Bursov et al. 1996; Parijskij et al. 1996; Soboleva et al. 2010; Zhelenkova et al. 2017; Zhelenkova & Majorova et al. 2018);

"new": The spectral index α^{3000}_{340} is determined in the frequency range 340–3000 MHz using linear approximation of VCSS, RACS-low, RACS-mid, NVSS, VLASS data, as well as from Tung

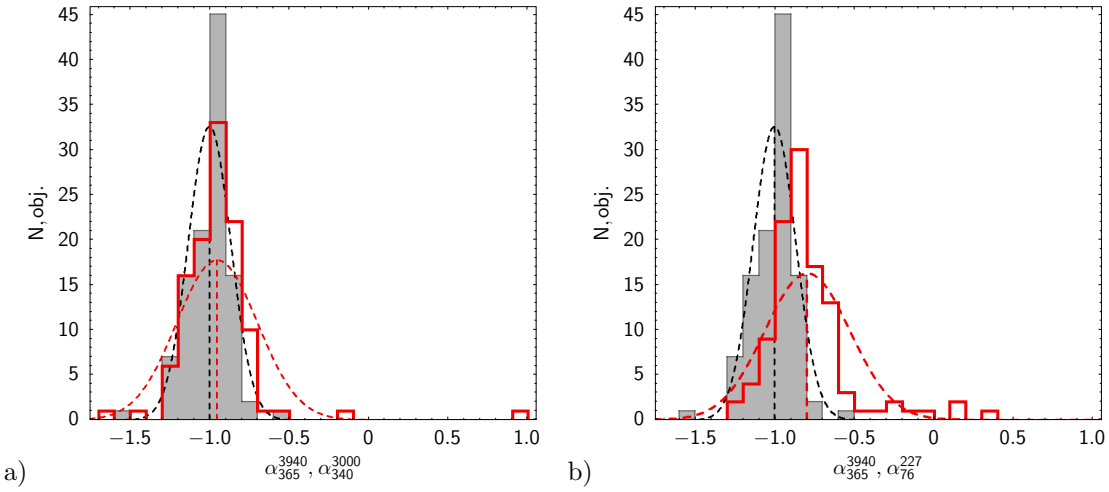

Figure 5. Comparison of spectral indices α_{365}^{3940} calculated using linear approximation of "old" data, α_{340}^{3000} — of "new" data, and α_{74}^{231} — of "glm" data for radio sources of the Big Trio program. Distributions and their approximation by Gaussians for spectral indices: (a) α_{365}^{3940} (grey) and α_{340}^{3000} (red line); (b) distributions of spectral indices α_{365}^{3940} (grey) and α_{76}^{227} (red line).

et al. (2017); de Gasperin et al. (2018); Bruzewski et al. (2021); Gordon et al. (2023). The frequency range is chosen in such a way that it coincides to some extent with the range 365–3940 MHz;

"glm": α_{76}^{227} is calculated by linearly fitting the GLEAM data;

"all": Spectral indices α_{74} and α_{7700} are calculated by parabolic approximation of all available flux density data for each source, respectively, at frequencies of 74 and 7700 MHz. The spectral curvature parameter is calculated as SCP $= \alpha_{74} - \alpha_{7700}$. This parameter is often used to estimate the evolutionary stage of a radio source (Murgia et al. 2011).

We compared the spectral indices of the Big Trio program sources, which were calculated by linearly fitting the data from the "old", "new", and "glm" datasets. The histograms (see Fig. 5a) show a comparison of the old and new spectral indices α_{365}^{3940} and α_{340}^{3000}. The index distributions do not differ significantly from each other. When comparing the α_{365}^{3940} with α_{76}^{227} (see Fig. 5b), it is noticeable that α_{76}^{227} indices are shifted toward flatter spectra.

According to the above-mentioned publication Soboleva et al. (1994), 83 out of the 88 sources presented there, which were included in the Big Trio, had $\alpha_{\rm all} \leq -0.9$ (i.e. 94 %). If we stick to the same frequency range, then for the "old" data set, 90 (80 %) out of 112 sources have $\alpha_{\rm all} \leq -0.9$, and for the "new" set, 79 (70 %) out of 113 sources have such a spectral index. For the spectral indices determined from the "glm" set, it turns out that 39 sources have $\alpha_{\rm all} \leq -0.9$, which is 35 % of the sample. The low percentage of steep-spectrum sources whose spectral index was determined from GLEAM data can be explained by the spectrum roll-off at low frequencies due to electron ageing.

Next, we divided the radio sources into two subsamples. Subsample (I) included radio sources that do not have a peak in the spectrum; the curvature of the continuous spectrum, determined by the SCP parameter, lies in the range 0.0–0.5 (Murgia et al. 2011), and the variability index $|V_{340}^{cc} < 3|$. For sources included in this subsample, we believe that the linear approximation of the continuous spectrum will not depend strongly on the different data sets on the basis of which the spectral index is determined. The subsample included 55 sources. The second subsample (II) includes all other sources that were not included in subsample (I).

When comparing subsamples (I) and (II), the discrepancy in the spectral index distributions is particularly noticeable for subsample (II) (see Fig. 6). In subsample (I), the number of sources with $\alpha \leq -0.9$, calculated using spectral indices from the "old" and "new" datasets, remained virtually

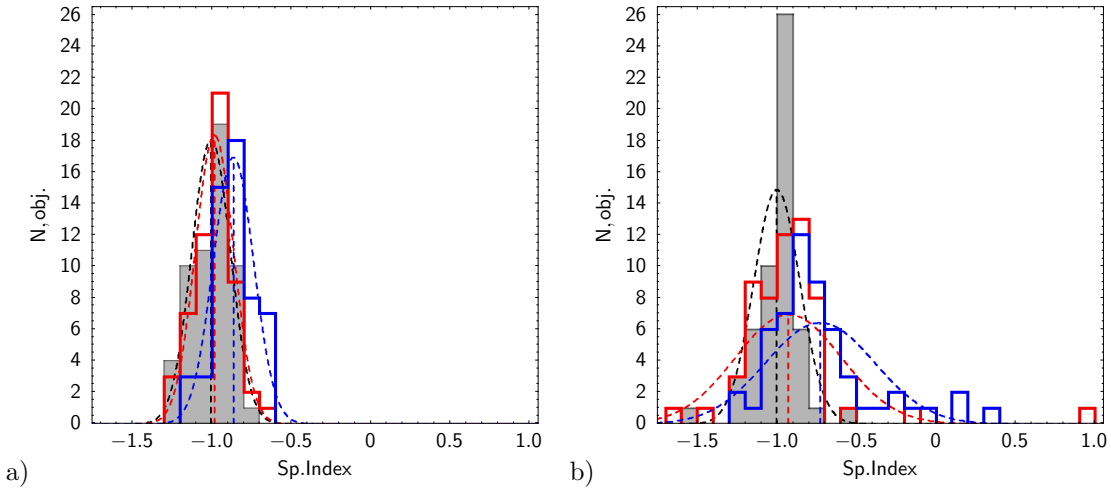

Figure 6. Comparison of the distributions of spectral indices α_{365}^{3940} (marked in grey), α_{340}^{3000} (marked in red), and α_{76}^{227} (marked in blue) and their Gaussian approximations for (a) subsample (I) and (b) subsample (II).

Table 2. Comparison of spectral indices of subsamples (I) and (II). Sp.Ind. — mean and RMS of distribution; Median — median of distribution; SS — number of sources with steep spectra ($\alpha \leq -0.9$)

	Sp.Ind.	Median	SS, obj
(I)	$\alpha_{365}^{3940} = -1.05 \pm 0.10$	-1.03	44
(II)	$\alpha_{365}^{3940} = -1.04 \pm 0.12$	-1.00	46
(I)	$\alpha_{340}^{3000} = -1.03 \pm 0.09$	-1.01	43
(II)	$\alpha_{340}^{3000} = -1.08 \pm 0.15$	-1.06	36
(I)	$\alpha_{76}^{227} = -0.99 \pm 0.06$	-0.96	22
(II)	$\alpha_{76}^{227} = -1.04 \pm 0.09$	-1.03	17

unchanged (see Table 2). However, in subsample (II), the number of such sources decreased from 46 (based on the "old" data) to 36 (based on the "new" data), and the number of sources with $\alpha_{76}^{227} \leq -0.9$ is also lower than in subsample (I).

This can be explained by the fact that subsample (I) includes sources whose jets continue to receive power from the active nucleus. The situation is different in subsample (II). In addition to variable sources, it includes young radio sources, whose jets are in the initial stages of development, and fading sources, whose jets cease receiving power from the active nucleus. Thus, in subsample (II), the change in the continuous spectra – the shift of the entire spectrum to the low-frequency region and the roll-off of the spectrum at low frequencies – should occur more noticeably than in subsample (I).

6. Results

6.1. Morphology

For a well-studied sample of steep-spectrum sources of the Big Trio program, we refined the radio morphology using radio maps with angular resolutions ranging from 0.1″ to 2.5″.

Visual inspection of radio maps and cutouts from optical and infrared surveys revealed that some radio sources are not a single radio source, but consist of two sources located close to each other on the observational plane. There were six such objects, with four sources being formed from pairs of close radio sources, which are confirmed by the redshift of the hosts, the distance between which is about 60 kpc.

In addition to the FRII-type radio galaxies, which make up 72 % of the sample, there are 3 % of FRI-type galaxies, 11 % of the hybrid FRI/FRII type, and 18 % of point sources that cannot be resolved on the available radio maps. 27 % of the double sources have a core.

In six radio sources, the contribution of the core is more than 35 % and they can be classified as core-dominated triple radio sources. Three radio sources have double-double lobes. Thus, according to morphological features, 8 % of the sources in the sample show a restart of activity in the radio range.

The deformation of the radio lobes indicates interaction with the environment of the radio source at different distances from the active nucleus. Thus, wing-shaped lobes of the radio source indicate a sharp reorientation of the jet caused by the instability of the accretion disk, possibly caused by interaction with a nearby massive object. Hybrid radio lobes are explained by the inhomogeneity of the environment surrounding the radio galaxy. WATs indicate the presence of the radio source in a group or cluster of galaxies.

In the sample, we classified 12 sources as WRGs, 8 sources as WATs, and 4 sources as horseshoe-shaped and C-shaped. If we add another 8 FRI/FRII sources, then 20 % of the hosts in the sample[4] have neighbors or are located in a group or cluster of galaxies.

The sample includes two giant radio galaxies, as well as twenty-six compact radio sources with sizes from 0.7 to 19 kpc.

6.2. Variability

We compared the integral flux densities of radio sources at frequencies of 340–365 MHz, 1368–1400 MHz, 3900–3940 MHz, and 4850–5000 MHz. Of the 87 sources for which data are available in the VCSS and TXS catalogs, 44 % have variability indices $|V_{340}| > 3$. According to RACS and NVSS data, there are no variable sources in the sample. At frequencies of 3900–3940 MHz, 31 % of 101 radio sources have $V_{3940} > 3$, and at 4850–5000 MHz, 37 % of 93 objects have $V_{4850} > 3$.

We studied the VCSS and TXS data in more detail, since the maximum interval between mean epochs of the surveys is about 40 years. The presence of a large proportion of objects with $|V_{340} > 3|$ among the sources in the sample is explained, first of all, by the difference in the angular resolution of the surveys and, as a result, the contribution to the integrated flux density from nearby sources in S_{365}, as well as, as it turned out, an underestimated value of S_{340} for some double sources.

After the corrections were made, there are still 19 radio sources with $|V_{340} > 3|$. The sources with $|V_{340} > 3|$ may include sources with a peak in the spectrum and compact, rapidly evolving sources whose spectral maximum shifts to the low-frequency region. We assume that a time interval of about 4 decades is sufficient for such an evolution to be noticeable. Such sources turned out to be 11 %.

It is also possible that some sources have extended low surface brightness components that not are detected in the VCSS survey, but most likely detected in TXS and GLEAM. We did not consider this hypothesis in detail here.

Among the sources with the variability index $|V_{340}| > 3$ there may be variable sources. In the studied sample of sources suspected of variability, there were about 10 % of them. These are mainly compact radio quasars.

[4]Some radio sources may combine morphological features, for example DD and VAT.

6.3. Continuum spectra

We compared the spectral indices of the Big Trio sample sources obtained from spectra constructed by fitting data from several sets of integral flux densities, namely, data available before 1996 and data from new radio surveys.

Of the 113 sources, 90 sources have a two-frequency spectral index of $\alpha_{3940}^{365} \leq -0.9$, 79 sources have $\alpha_{3000}^{340} \leq -0.9$ according to new surveys VCSS, RACS and VLASS, and 39 sources have $\alpha_{227}^{76} \leq -0.9$ according to GLEAM data. Most likely, this is due to the addition of low-frequency GLEAM data. Although for some radio sources the change in spectrum may be caused by the evolution of the source, expressed in a shift of the peak or roll-off of the spectrum towards lower frequencies, which is noted by measurements of the flux density in various catalogues over an interval of up to forty years.

Acknowledgements The observations were carried out with the RATAN-600 scientific facility. This research has made use of the NASA/IPAC Extragalactic Database (NED), which is operated by the Jet Propulsion Laboratory, California Institute of Technology, under contract with the National Aeronautics and Space Administration; the CATS database available on the Special Astrophysical Observatory website.

References

Abbott T., Abdalla F., Allam S., et al., 2018, Astrophysical Journal Suppl., 239, 2, id. 18
Abbott T., Adamów M., Aguena M., et al., 2021, Astrophysical Journal Suppl., 255, 2, id. 20
Afanasiev V., Dodonov S., Moiseev A., et al., 2003, Astronomy Reports, 47, 5, p. 377
Afanasiev V. and Moiseev A., 2005, Astronomy Letters, 31, 3, p. 194
Aihara H., AlSayyad Y., Ando M., et al., 2019, Publications of the Astronomical Society of Japan, 71, 6, id. 114
Aihara H., AlSayyad Y., Ando M., et al., 2022, Publications of the Astronomical Society of Japan, 74, 2, p. 247
Aird J., Nandra K., Laird E., et al., 2010, Monthly Notices of the Royal Astronomical Society, 401, 4, p. 2531
Amirkhanyan V., Gorshkov A., Kapustkin A., et al., 1985, Soobshch. SAO, 47, p. 5
Andernach H., Jimenez-Andrade E., Willis A., 2021, Galaxies, 9, 4, id. 99
Bennett C., Lawrence C., Burke B., et al., 1986, Astrophysical Journal Suppl., 61, p. 1
Bera S., Sasmal T., Patra D., et al., 2022, Astrophysical Journal Suppl., 260, 1, id. 7
Berlin A., Bulaenko E., Golnev V., et al., 1981, Soviet Astronomy Letters, 7, p. 161
Berlin A., Gassanov L., GolNev V., et al., 1984, Soobshch. Spets. Astrofiz. Obs., 41, 84 pp.
Berlin A., Gassanov L., GolNev V., et al., 1984, Soobshch. Spets. Astrofiz. Obs., 42, 73 pp.
Binette L., Carignan C., Bolton J., et al., 1981, Australian Journal of Physics, 34, p. 407
Blanton E., Gregg M., Helfand D., et al., 2000, Astrophysical Journal, 531, 1, p. 118
Bonnarel F., Fernique P., Bienayme O., et al., 2000, Astronomy and Astrophysics Suppl., 143, p. 33
Broderick J., Bryant J., Hunstead R., et al., 2007, Monthly Notices of the Royal Astronomical Society, 381, 1, p. 341
Bruzewski S., Schinzel F., Taylor G., et al., 2021, Astrophysical Journal, 914, 1, id. 42
Bryant J., Johnston H., Broderick J., et al., 2009, Monthly Notices of the Royal Astronomical Society, 395, 2, p. 1099
Bursov N., Bulletin of the Special Astrophysical Observatory, 40, p. 128
Bursov N., Lipovka N., Soboleva N., et al., 1996, Bulletin of the Special Astrophysical Observatory, 42, p. 5
Carilli C., Rottgering H., van Ojik R., et al., 1997, Astrophysical Journal Suppl., 109, 1, p. 1
Carilli C., Gnedin N., Owen F., 2002, Astrophysical Journal, 577, 1, p. 22
Cohen A., Lane W., Cotton W., et al., 2007, Astronomical Journal, 134, 3, p. 1245
Condon J., Cotton W., Greisen E., et al., 1998, Astronomical Journal, 115, 5, p. 1693
Cutri R., Wright E., Conrow T., et al., 2012, Explanatory Supplement to the WISE All-Sky Data Release Products, p. 1
De Breuck C., van Breugel W., Röttgering H., et al., 2000, Astronomy and Astrophysics Suppl., 143, p. 303
De Breuck C., Hunstead R., Sadler E., et al., 2004, Monthly Notices of the Royal Astronomical Society, 347, 3, p. 837
De Breuck C., Klamer I., Johnston H., et al., 2006, Monthly Notices of the Royal Astronomical Society, 366, 1, p. 58
De Breuck C., Seymour N., Stern D., et al., 2010, Astrophysical Journal, 725, 1, p. 36
de Gasperin F., Intema H. T., Frail D., 2018, Monthly Notices of the Royal Astronomical Society, 474, 4, p. 5008
Dodonov S., Pariiskii Yu., Goss W., et al., 1999, Astronomy Reports, 43, 5, p. 275
Douglas J., Bash F., Torrence G., et al., 1980, University of Texas - Publications in Astronomy, 17, p. 1
Douglas J., Bash F., Bozyan F., et al., 1996, Astronomical Journal, 111, p. 1945

Drouart G., De Breuck C., Vernet J., et al., 2012, Astronomy and Astrophysics, 548, id. A45
Duchesne S., Grundy J., Heald G., et al., 2024, Publications of the Astronomical Society of Australia, 41, id. E003
Falder J., Stevens J., Jarvis M., et al., 2010, Monthly Notices of the Royal Astronomical Society, 405, 1, p. 347
Fanaroff B. and Riley J., 1974, Monthly Notices of the Royal Astronomical Society, 167, p. 31
Fletcher A., Conner S., Crawford F., et al., 1996, Astronomy Reports, 40, 6, p. 759
Galametz A., Stern D., De Breuck C., et al., 2012, Astrophysical Journal, 749, 2, id. 169, p. 12
Gopal-Krishna and Wiita, P., 2000, Astronomy and Astrophysics, 363, p. 507
Gordon Y., Rudnick L., Andernach H., et al., 2023, Astrophysical Journal Suppl., 267, 2, id. 37
Goss W., Parijskij Yu., Soboleva N., et al., 1992, Astronomicheskii Zhurnal, 69, p. 673
Goss W., Pariiskii Y., Soboleva N., et al., 1992, Soviet Astronomy, 36, 4, p. 343
Gregory P., Scott W., Douglas K., et al., 1996, Astrophysical Journal Suppl., 103, p. 427
Griffith M., Wright A., Burke B., et al., 1995, Astrophysical Journal Suppl., 97, p. 347
Hale C., McConnell D., Thomson A., et al., 2021, Publications of the Astronomical Society of Australia, 38, id. E058
Haring N. and Rix H.-W., 2004, Astrophysical Journal, 604, 2, p. L89
Helfand D., White R., Becker R., 2015, Astrophysical Journal, 801, 1, id. 26
Hopkins A. and Beacom J., 2006, Astrophysical Journal,651, 1, p. 142
Hopkins P., Hernquist L., Cox T., et al., 2006, Astrophysical Journal Suppl., 163, 1, p. 50
Huang W., Olsen K., Fitzpatrick M., et al., 2020, ADSS XXVII. ASP Conf. Ser., 522, p. 153
Hurley-Walker N., Callingham J., Hancock P., et al., 2017, Monthly Notices of the Royal Astronomical Society, 464, 1, p. 1146
Intema H., Jagannathan P., Mooley K., et al., 2017, Astronomy and Astrophysics, 598, id. A78
Kapahi V. and Kulkarni V., 1990, Astronomical Journal, 99, p. 1397
Kapinska A., Terentev I., Wong O., et al., 2017, Astronomical Journal,154, 6, id. 253
Kopylov A., Goss V., Pariiskii Yu., et al., 1995, Astronomy Reports, 39, 5, p. 543
Kopylov A., Goss W., Parijskij Yu., et al., 2006, Astronomy Letters, 32, 7, p. 433
Kumari S. and Pal S., 2024, Astronomy and Astrophysics, 683, id. A175
Lane W., Cotton W., van Velzen S., et al., 2014, Monthly Notices of the Royal Astronomical Society, 440, 1, p. 327
Lara L., Cotton W., Feretti L., et al., 2001, Astronomy and Astrophysics, 370, p. 409
Large M., Cram L., Burgess A., 1991, Observatory, 111, p. 72
Lawrence A., Warren S., Almaini O., et al., 2007, Monthly Notices of the Royal Astronomical Society, 379, 4, p. 1599
Lucas P., Hoare M., Longmore A., et al., 2008, Monthly Notices of the Royal Astronomical Society, 391, 1, p. 136
Magorrian J., Tremaine S., Richstone D., 1998, Astronomical Journal, 115, 6, p. 2285
Majorova E., Zhelenkova O., Temirova A., 2015, Astrophysical Bulletin, 70, 1, p. 33
Majorova E. and Zhelenkova O., 2012, Astrophysical Bulletin, 67, 3, p. 318
Marecki A., Thomasson P., Mack K.-H., et al., 2006, Astronomy and Astrophysics, 448, 2, p. 479
Marocco F., Eisenhardt P., Fowler J., et al., 2021, Astrophysical Journal Suppl., 253, 1, id. 8
Mayo J., Vernet J., De Breuck C., et al., 2012, Astronomy and Astrophysics, 539, id. A33
Miley G. and De Breuck C., 2008, Astronomy and Astrophysics Review, 15, 2, p. 67
Missaglia V., Massaro F., Capetti A., et al., 2019, Astronomy and Astrophysics, 626, id. A8
Murgia M., Parma P., Mack K., 2011, Astronomy and Astrophysics, 526, id. A148
Nesvadba N., Lehnert M., De Breuck C., et al., 2008, Astronomy and Astrophysics, 491, 2, p. 407
Norris R., Crawford E., Macgregor P., 2021, Galaxies, 9, 4, id. 83
Orienti M. and Dallacasa D., 2021, Astronomische Nachrichten, 342, 1151, p. 1151
Pariiskij Yu., Bursov N., Lipovka N., et al., 1991, Astronomy and Astrophysics Suppl., 87, p. 1
Pariiskij Yu., Bursov N., Lipovka N., et al., 1992, Astronomy and Astrophysics Suppl., 96, p. 583
Parijskij Yu., Goss W., Kopylov A., et al., 1995, Bulletin of the Special Astrophysical Observatory, 40, p. 5
Parijskij Y., Goss W., Kopylov A., et al., 1996, Bulletin of the Special Astrophysical Observatory, 40, p. 5
Parijskij Yu., Goss W., Kopylov A., et al., 2000, Astronomical and Astrophysical Transactions, 19, 3, p. 297
Parijskij Yu., Kopylov A., Temirova A., et al., 2010, Astronomy Reports, 54, 8, p. 675
Parijskij Yu., Thomasson P., Kopylov A., et al., 2014, Monthly Notices of the Royal Astronomical Society, 439, 3, p. 2314
Peters W., Polisensky E., Brisken W., et al., 2021, American Astronomical Society meeting N237, Bull. of the American Astronomical Society, 53, 1, e-id 2021n1i211p06
Planck Collaboration, 2020, Astronomy and Astrophysics, 641, id. A6
Polisensky E., Lane W., Hyman S., et al., 2016, Astrophysical Journal, 832, 1, id. 60
Pursimo T., Nilsson K., Teerikorpi P., et al., 1999, Astronomy and Astrophysics Suppl., 134, p. 505
Rawlings J., Seymour N., Page M., et al., 2013, Monthly Notices of the Royal Astronomical Society, 429, 1, p. 744
Roettgering H., Lacy M., Miley G., et al., 1994, Astronomy and Astrophysics Suppl., 108, p. 79
Roettgering H., van Ojik R., Miley G., et al., 1997, Astronomy and Astrophysics, 326, p. 505
Rudnick L. and Owen F., 1976, Astrophysical Journal, 203, p. L107
Saikia D., Konar C., Kulkarni V., 2006, Monthly Notices of the Royal Astronomical Society, 366, 4, p. 1391
Sasmal T., Bera S., Pal S., et al., 2022, Astrophysical Journal Suppl., 259, 2, id. 31
Saxena A., Jagannathan P., Röttgering H., et al., 2018, Monthly Notices of the Royal Astronomical Society, 475, 4, p. 5041
Saxena A., Marinello M., Overzier R., et al., 2018, Monthly Notices of the Royal Astronomical Society, 480, 2, p. 2733

Saxena A., 2019, PhD thesis, Leiden University
Schoenmakers A., de Bruyn A., Rottgering H., et al., 2000, Monthly Notices of the Royal Astronomical Society, 315, 2, p. 371
Seymour N., Stern D., De Breuck C., et al., 2007, Astrophysical Journal Suppl., 171, 2, p. 353
Shimmins A., Bolton J., Wall J., 1974, Australian Journal of Physics, Astrophysical Suppl., 34, p. 63
Soboleva N., Pariiskii Yu., Naugolnaya M., 1994, Astronomicheskii Zhurnal, 71, p. 684
Soboleva N., Majorova E., Zhelenkova O., et al., 2010, Astrophysical Bulletin, 65, 1, p. 42
Stevens J., Ivison R., Dunlop J., et al., 2003, Nature, 425, 6955, p. 264
Stevens J., Jarvis M., Coppin K., et al., 2010, Monthly Notices of the Royal Astronomical Society, 405, 4, p. 2623
Stroe A, Catlett V., Harwood J., et al., 2022, Astrophysical Journal, 941, 2, id. 136
Taylor M., 2005, ADASS XIV, ASP Conf. Ser, 347, p. 29
Tielens A., Miley G., Willis A., 1979, Astronomy and Astrophysics Suppl., 35, p. 153
Tung A., Kothes R., Landecker T., et al., 2017, Astronomical Journal, 154, 4, id. 156
Verkhodanov O., Erukhimov B., Monosov M., et al., 1993, Bulletin of the Special Astrophysical Observatory, 36, p. 132
Verkhodanov O., Kopylov A., Zhelenkova O., et al., 2002, Proc. of IAU Symposium 199, p. 247
Verkhodanov O. V., Trushkin S. A., Andernach H., et al., 2005, Bulletin of Special Astrophysical observatory, 58, p. 118
Vernet J., Fosbury R., Villar-Martín M., et al., 2001, Astronomy and Astrophysics, 366, p. 7
Wang W., Wylezalek D., De Breuck C., et al., 2021, Astronomy and Astrophysics, 654, id. A88
Wenger M., Ochsenbein F., Egret D., et al., 2000, Astronomy and Astrophysics Suppl., 143, p. 9
White S. and Rees M., 1978, Monthly Notices of the Royal Astronomical Society, 183, p. 341
Willis A., Strom R., Wilson A., 1974, Nature, 250, 5468, p. 625
Wright A. and Otrupcek R., 1990, PKS Catalog
Wright A., Griffith M., Burke B., 1994, Astrophysical Journal Suppl., 91, p. 111
Yang X., Joshi R., Gopal-Krishna, et al., 2019, Astrophysical Journal Suppl., 245, 1, id. 17
Zhelenkova O., Soboleva N., Temirova A., et al., 2017, Astrophysical Bulletin, 72, 2, p. 150
Zhelenkova O. and Majorova E., 2018, Astrophysical Bulletin, 73, 2, p. 142